Available online at www.sciencedirect.com
SCIENCE DIRECT®
PERGAMON
International Journal of Heat and Mass Transfer 46 (2003) 4083–4095
International Journal of HEAT and MASS TRANSFER
www.elsevier.com/locate/ijhmt

Numerical analysis of wave-type heat transfer propagating in a thin foil irradiated by short-pulsed laser

Eiji Hoashi [a,*], Takehiko Yokomine [b], Akihiko Shimizu [b], Tomoaki Kunugi [c]

[a] *Department of Nuclear System Analysis Technology R&D, Power & Industrial System Research & Development Center, Power System & Services Company, Toshiba Corporation, 4-1 Ukishima-cho, Kawasaki-ku, Kawasaki, Kanagawa 210-0862, Japan*
[b] *Division of Energy Engineering and Science, Interdisciplinary Graduate School of Engineering Sciences, Kyushu University, 6-1 Kasuga-kouen, Kasuga, Fukuoka 816-8580, Japan*
[c] *Department of Nuclear Engineering, Graduate School of Engineering, Faculty of Engineering, Kyoto University, Yoshida, Sakyo-ku, Kyoto 606-8501, Japan*

Received 3 April 2002; received in revised form 12 February 2003

Abstract

This paper presents a numerical simulation of wave-type heat transfer phenomena propagating in an aluminum thin foil irradiated by a pulsed laser using the cubic interpolated propagation method coupled with a thermo-convective model. We did not use the two-step model and dual-phase lag model, which are generally known as the non-Fourier heat conduction law, but wave-type heat transfer phenomena could be observed by our method. The main characteristic of the method is to solve the governing equation including the equation of continuity, the equation of motion, the equation of energy and the equation of state. It is found that when the pulse duration is under the order of picosecond, the pure heat conduction is hardly observed and heat transfer toward the inside of materials occurs only by a thermal shock wave. The heat conduction mode after pulse laser irradiation is strongly dependent upon the value of total incident laser energy density E_{in} and the threshold value for pure heat conduction is 5.0×10^4 J/m^2 for an aluminum.

1. Introduction

Although the high-power pulsed laser was originally developed for laser fusion applications, it has been applied to various engineering problems, for example, microscale or nanoscales processing and investigation of extreme properties under high-temperature and high-pressure conditions. In practical applications, the heat transfer mechanisms in materials subjected to a high heat flux for a very short-time heating pulse have been of great interest, for example, in conjunction with the improvement of accuracy of laser processing. However, since the scales of time and size of these phenomena cover the region from micro to macro and it is difficult to obtain dynamic information on materials by experiments, it is important to elucidate them by using numerical simulations.

From a microscopic point of view, the mechanism of heat transfer in a metal material is governed by phonon–electron interactions, the collisions between phonons and the energy transfer by free electrons. In the study of a very short-time phenomenon, we have to consider the mean free path of phonons and free electrons, the excitation process of atoms by an electron and the mechanism of exchange of energy between phonons and free electrons. Therefore, the heat transfer velocity must be a finite value. In heat conduction theory from a macroscopic perspective, however, there is inconsistency in that the heat transfer velocity has an infinite value. Generally, it has been mentioned that heat transfers as a wave rather than a diffusion in materials subjected to heat load during a very short time. This fact have been investigated by many researchers since Cattaneo [1] and Vernotte [2,3] proposed wave-type heat transfer theory including the CV equation, which is an energy balance

* Corresponding author. Tel.: +81-44-288-8150; fax: +81-44-270-1806.
E-mail address: eiji2.hoashi@toshiba.co.jp (E. Hoashi).

0017-9310/03/$ - see front matter © 2003 Elsevier Ltd. All rights reserved.
doi:10.1016/S0017-9310(03)00225-4

Nomenclature

B	isothermal bulk modulus (N/m^2)	s	specific entropy (J/kg K)
C_v	specific heat at constant volume $= \partial e/\partial T_\rho$ (J/kg K)	t	time (s)
		t_g	Gaussian distribution time (s)
d	depth (m)	t_p	pulse duration (s)
e	internal energy per unit mass (J/kg)	T	temperature (K)
g	acceleration of gravity (m/s^2)	u	velocity (m/s)
G	shear modulus (N/m^2)	v	specific volume (m^3/kg)
E_{in}	total incident laser energy density (J/m^2)	x	spatial coordinates (m)
F	volume force generated by surface tension (N/m^3)	Y_0	yield strength (N/m^2)
		α	absorption coefficient (1/m)
I_0	initial incident laser energy intensity (W/m^2)	β	isobaric volumetric expansion coefficient (1/K)
I	laser energy intensity at the depth d (W/m^2)		
N_c	a number of contour line	δ	Kronecker delta
P	pressure (N/m^2)	ε	strain tensor
P_{TH}	$T(\partial P/\partial T)_\rho$ (N/m^2)	ϕ	density function
Q	volume heat source (W/m^3)	κ	curvature of interface between different materials
r	distance from beam center (m)		
r_c	position of beam center (m)	λ	thermal conductivity (W/m K)
r_g	Gaussian beam radius (m)	ρ	density (kg/m^3)
S	stress (N/m^2)	σ	surface tension coefficient (N/m^3)

equation considering a thermal relaxation time according to Fourier's law. The principal method is to solve the hyperbolic heat conduction equation (HHCE) derived from the energy balance equation. Chandrasekharaiah [4] investigated wave-type heat transport using thermoelasticity theory, which was approached by introducing a flux-rate into the heat conduction law and by including temperature-rate among constitutive variables. Tzou [5] succeeded in simulation of heat source generated due to plastic deformation at a tip of a dynamically propagating crack in a metal using HHCE. Furthermore, Özisik and Tzou [6] described physical interpretation according to the CV equation, though the theoretical basis was insufficient. They recently proposed the dual-phase-lag (DPL) model extended from HHCE [7,8], in which the phase lag of both the heat flux and the temperature gradient were considered. Mitra et al. [9] showed experimental evidence of hyperbolic heat conduction and Kaminski [10] considered the physical meaning of the constant τ in HHEC and discussed experimental determination of τ. Tang and Araki [11,12] analyzed temperature profile in finite medium irradiated by short-pulsed laser using HHCE and indicated a condition such that thermal shock wave can penetrate to the back surface of target material. Moreover, They also extended DPL model to elastic material [13]. As well as Tang et al., Sumi [14] investigated the temperature behavior in finite medium irradiated by short-pulsed laser using the equation of motion, the constitutive equation and HHCE based on generalized thermoelasticity theory. In these studies, however, interrelation between temperature and other properties, e.g., pressure and density, is not considered and thus the result is confined to physical interpretation only. Generally, in the formulation of HHCE, the thermal relaxation time τ is assumed to be constant in a medium. However, this is equal to the assumption that the material has no compressibility because density is related in the definition of τ. In materials under a short-pulse thermal load, the heating time is shorter than the time required for thermal expansion to occur. In this case, pressure and temperature rapidly rise in the energy deposition region and shock wave propagates toward the inside of the material, which is brought about by the reaction force due to an explosive thermal expansion of the energy deposition region. In these processes, a dilatation and compression process must be naturally considered and thus it is insufficient to analyze these phenomena as practical engineering problems using the assumption of incompressibility. Ozoe et al. [15] considered this point and analyzed the interference of shock wave with wave reflected by the opposite surface in fluid between two walls, in which one wall is subjected to pulsed heating. They used a thermo-convective model, which consists of the equations of continuity, motion and energy and the adequate equation of state (EOS). Moreover, Churchill et al. [16] compared thermo-convective model with HHCE and described how this model can provide an adequate representation of the heat transfer as a wave with sufficient accuracy for practical purposes. However, their

analysis is also restricted to a homogeneous material with no phase change process and the ideal fluid because an adequate EOS is unavailable. Kuznetsov [17,18] analyzed a wave of temperature difference between solid and fluid phases in a porous packed bed using a perturbation technique of the full energy equation for fluid and solid in one- and two-dimensional systems. In his analyses, an incompressibility and no phase change are also assumed and interrelation between temperature and other properties is neglected. Since in the case of material subjected to high-energy flux, a phase change occurs, such as melting, their analysis is insufficient for practical phenomena as well as HHCE.

On the other hand, the cubic interpolated propagation (CIP) method proposed by Yabe et al. [19], which enables accurate solving of the convective term by interpolating information on physical quantity between grids with cubic-polynomial, has been developed as a method which can solve discontinuous region of physical quantity while keeping relative numerical stability. Since the CIP method can be easily extended to mixture field of more than two kinds of materials and can consider compressibility and incompressibility simultaneously, there have been numerous applications to phenomena with phase change and multiphase flow. Yabe [20] analyzed laser-induced evaporation and welding process using the CIP method and the results provided an interpretation of cutting and keyhole creation processes. Fujii et al. [21] and Utsumi et al. [22] also analyzed laser-driven shock wave in a silver thin foil irradiated by high-power ultra-short-pulsed laser using the CIP method. However, they investigated only the profile of pressure and density, and the temperature was obtained from the EOS table by using the calculated pressure and density. In their paper, the wave-type heat transfer was not referred. We will apply the CIP method and investigate the generation and propagation of wave-type heat transfer, that is, the so-called *thermal shock wave* in aluminum thin foil irradiated by a pulsed laser.

2. Numerical model

In the CIP method, transport equations of physical quantities f are split into two steps, advection phase and non-advection phase, as follows.

$$\frac{\partial f}{\partial t} + u_i \frac{\partial f}{\partial x_i} = f' \tag{1}$$

where f' presents the right-hand side of governing equations and subscript i is the index describing the axis of the coordinates. In CIP method, it is possible to solve the equation explicitly with the finite difference method in non-advection phase. A characteristic of the CIP method is to solve the first spatial derivative.

The model consists of the equations of continuity, motion and energy and appropriate EOS as follows:

$$\frac{\mathrm{D}\rho}{\mathrm{D}t} = -\rho \frac{\partial u_i}{\partial x_i} \tag{2}$$

$$\rho \frac{\mathrm{D}u_i}{\mathrm{D}t} = -\frac{\partial P}{\partial x_i} + \frac{\partial S_{ij}}{\partial x_j} + F_i + \rho g_i \tag{3}$$

$$\rho \frac{\mathrm{D}e}{\mathrm{D}t} = -P \frac{\partial u_i}{\partial x_i} + S_{ij} \frac{\partial u_i}{\partial x_j} + \frac{\partial}{\partial x_i}\left(\lambda \frac{\partial T}{\partial x_i}\right) + Q \tag{4}$$

$$P = P(\rho, T), \quad e = e(\rho, T) \tag{5}$$

Here, subscript j is also the index describing the axis of each coordinates as well as i.

For surface tension, we apply the continuum surface force (CSF) model proposed by Brackbill et al. [23]. In the CSF model, a discontinuity problem of interface is represented as transition region of finite thickness, and thus the surface tension represented as surface force can be changed to volume force. It is assumed that the properties of interface are continuous in this transition region, and the curvature of interface required to solve volume force is described using a gradient of "color function". On the other hand, in the CIP method, a density function ϕ is introduced to distinguish the materials in a field where multiphase or different materials exist [24]. The density function takes a value only from 0 to 1 and in each grid.

$$\sum_n \phi_n = 1 \tag{6}$$

where subscript n is the number of the phase or material. For physical quantity having spatial discontinuity, we can calculate the physical quantity with this density function as follows:

$$f = \sum_n \phi_n f_n \tag{7}$$

Since the color function required in the CSF model can be considered as the density function in the CIP method, introduction of the CSF model to the CIP method is easy. In the CSF model, the volume force F is written using the density function as follows:

$$F = \sigma\kappa \frac{\nabla\phi}{[\phi]} \tag{8}$$

where $[\phi] = \phi_2 - \phi_1$, which subscripts, 1 and 2, are the numbers of materials.

For the stress S, we apply a viscous elastic–plastic model, in which the elastic–plastic model proposed by Wilkins [25] and Xiao and Yabe [26] is applied in solid region and the stress term is regarded as the viscous term in fluid region. In the elastic–plastic model, the stress is developed by the following equation:

$$\frac{\partial S_{ij}}{\partial t} = 2G\left[\frac{1}{2}\left(\frac{\partial u_i}{\partial u_j} + \frac{\partial u_j}{\partial u_i}\right) - \frac{1}{3}\varepsilon_{kk}\delta_{ij}\right] \tag{9}$$

When the stress satisfies the von Mises condition as follows:

$$S_{ij} \cdot S_{ij} \geqslant \frac{2}{3} Y_0^2 \tag{10}$$

The stress can be modified as plastic deformation using the following equation:

$$S_{ij} = \sqrt{\frac{2}{3}} \frac{Y_0}{\sqrt{S_{ij} \cdot S_{ij}}} S_{ij} \tag{11}$$

The energy contribution by laser irradiation is considered as a volumetric heat source in the equation of energy. The absorption of laser energy is usually described by Beer's law,

$$I = I_0 \exp(-\alpha d) \tag{12}$$

Most lasers have profiles of Gaussian distribution in both time and space. The distribution of light source forms Gaussian distribution in every propagation path, and the distribution changes only when laser is focused by lens and is guided by mirror. In this study, we use laser with Gaussian distribution.

$$I(r,t,d) = I_0 \exp\left[-\alpha d - 2\frac{(t-2t_g)^2}{t_g^2} - 2\frac{(r-r_c)^2}{r_g^2}\right] \tag{13}$$

Volumetric heat source Q in Eq. (4) is given by

$$Q = Q(r,t,d) = \frac{I(r,t,d)}{d} \tag{14}$$

In this study, the energy transferred by radiation and interaction of laser driven plasma is not considered and the absorption coefficient is 1.0×10^7 m^{-1} under the assumption that the wavelength of laser is 532 nm for second-harmonic generation of Q-switching Nd:YAG laser.

As EOS, we used data from SESAME EOS data library [27] as well as Utsumi and Sasaki [22]. In SESAME, pressure, internal energy and Helmholtz free energy are prepared as functions of temperature and density, and the first derivative for each independent variable can be calculated by SESAME.

If v is a specific volume and s specific entropy, the total differential can be expressed as

$$\mathrm{d}e = -P\,\mathrm{d}v + T\,\mathrm{d}s \tag{15}$$

When $s = s(v,T)$, Eq. (15) is changed into

$$\begin{aligned}\mathrm{d}e &= -P\,\mathrm{d}v + T\left\{\left(\frac{\partial s}{\partial T}\right)_v \mathrm{d}T + \left(\frac{\partial s}{\partial v}\right)_T \mathrm{d}v\right\} \\ &= T\left(\frac{\partial s}{\partial T}\right)_v \mathrm{d}T + \left\{-P + T\left(\frac{\partial s}{\partial v}\right)_T\right\}\mathrm{d}v\end{aligned} \tag{16}$$

Substituting the Maxwell relation

$$\left(\frac{\partial s}{\partial v}\right)_T = \left(\frac{\partial P}{\partial T}\right)_v \tag{17}$$

and

$$T = \left(\frac{\partial e}{\partial s}\right)_T \tag{18}$$

into Eq. (16), the total differential of internal energy is obtained as

$$\mathrm{d}e = \left(\frac{\partial e}{\partial T}\right)_v \mathrm{d}T + \left\{-P + T\left(\frac{\partial P}{\partial T}\right)_v\right\}\mathrm{d}v \tag{19}$$

Eq. (19) can be rewritten by

$$\mathrm{d}e = C_v\,\mathrm{d}T + \{-P + P_{\mathrm{TH}}\}\left(-\frac{1}{\rho^2}\right)\mathrm{d}\rho \tag{20}$$

where $C_v = (\partial e/\partial T)_\rho$ and $P_{\mathrm{TH}} = T(\partial P/\partial T)_\rho$. From Eqs. (2), (4) and (20), the heat conduction equation is derived as follows:

$$\rho C_v \frac{\mathrm{D}T}{\mathrm{D}t} = -P_{\mathrm{TH}}\frac{\partial u_i}{\partial x_i} + S_{ij}\frac{\partial u_i}{\partial x_j} + \frac{\partial}{\partial x_i}\left(\lambda\frac{\partial T}{\partial x_i}\right) + Q \tag{21}$$

We use Eqs. (2), (3), (21) and (5) as governing equations. Here, the isobaric volumetric expansion coefficient β and the isothermal bulk modulus B are defined as follows:

$$\beta \equiv -\frac{1}{\rho}\left(\frac{\partial \rho}{\partial T}\right)_P, \quad B \equiv \rho\left(\frac{\partial P}{\partial \rho}\right)_T \tag{22}$$

Thus, P_{TH} can be considered as follows:

$$P_{\mathrm{TH}} = T\beta B \tag{23}$$

Namely, the first term of the right-hand side in Eq. (21) expresses an energy dissipation due to generation of thermal stress by temperature difference with neighbor regions.

3. Analytical system

Fig. 1 shows the two-dimensional simulation system. We consider an aluminum thin foil as a target material and it has a thickness and a width, 10 μm×20 μm, respectively. The region of upper aluminum thin foil is filled with air assumed to be ideal gas and the total calculation system size is 20 μm×20 μm. The initial conditions of the pressure and temperature are 0.1 MPa and 500 K, respectively, and the density is calculated from EOS as the value corresponding to 0.1 MPa and 500 K over the system. Because SESAME is basically provided for a high temperature region, the accuracy in

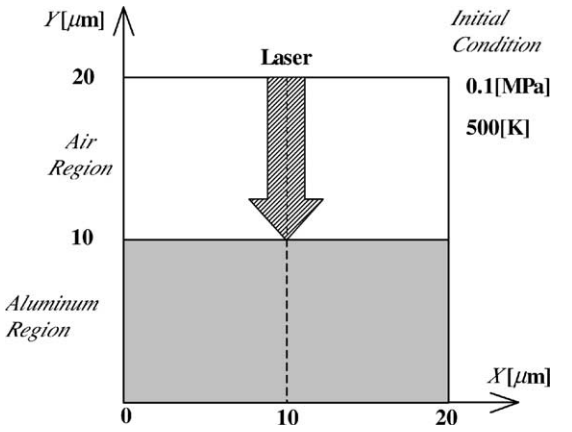

Fig. 1. Simulation system. The size is 20 μm×20 μm and the center of laser radius is located at $X = 10$ μm. Initial condition is $P_0 = 0.1$ MPa, $T_0 = 500$ K and ρ_0 of both regions is the value corresponding to P_0 and T_0.

the vicinity of room temperature is insufficient. In the present study, thus, the initial temperature is set to a relatively high value, 500 K. In the simulations, we treated a pulse duration, t_p, and an initial incident laser energy intensity, I_0, as parameters, which are considered in the ranges of 0.5–100 ps and 1.0×10^{16}–1.0×10^{17} W/m^2, respectively.

4. Results and discussion

Figs. 2–4 show temperature distributions within an aluminum thin foil. The pulse duration t_p is 1.0 ps in Case 1, 10.0 ps in Case 2, 100.0 ps in Case 3 with the common value of $I_0 = 5.0 \times 10^{16}$ W/m^2, respectively. In Figs. 2 and 3, (a) is the temperature distribution at 0.1 ns, (b) at 0.5 ns and (c) at 1.0 ns, and in Fig. 4, (a) is the temperature distribution at 0.09 ns, (b) at 0.39 ns and (c) at 0.76 ns. A number of a contour line for a temperature, N_c, is 400 and the display range of the contour line is shown in the figures.

As shown in Fig. 2, the thermal shock wave propagates toward the inside of a thin foil and it has been simulated that the propagation velocity is supersonic by authors [28]. Though the surface temperature is raised to over 1000 K, the temperature rise is small at the depth of about 2 μm from the surface in the center of X-direction. In Fig. 3, there is continuous and gradual temperature distribution under a high-temperature region at the surface. The pattern in Fig. 3 indicates that the conduction transport of heat is dominant. Generally, in a laser processing, a region subjected to deformation and transmutation by heat load is referred to as a heat affected zone and it is spread by heat conduction. As shown in Fig. 2, it is found that heat conduction hardly occurs and there is no spread of the heat affected zone in the case of using ultra-short-pulsed laser of picosecond order. It is generally considered that the heat affected zone does not occur when the pulse duration is shorter than the characteristic time of a specimen for pure heat conduction. When heat load is applied to material by an ultra-short-pulsed laser, the energy deposition takes place in very short time compared to the thermo-mechanical relaxation time, which is the shortest possible time for a thermal expansion to occur. The order of the time is r/c, in which r is the deposition range and c is the sound speed in solid [29], and here it is called a thermal expansion time t_r. In this study, since $r = 1.0 \times 10^{-7}$ m and $c = 6420$ m/s, $t_r = 1.56 \times 10^{-11}$ s. The thermal expansion time is equivalent to the characteristic time and the pulse duration of picosecond order is shorter than t_r. Thus, the spread of the heat affected zone doesn't become large when the pulsed laser with a duration of a range shorter than picosecond is used. As shown in Fig. 3, it is found that the thermal shock wave propagates faster than thermal diffusion by heat conduction and heat transfers to deeper region of thin foil by the thermal shock wave, which is isotropically spread in a semicircle except for a neighboring region of the surface. Heat transfer by the thermal diffusion is damped at an early stage. As shown in Fig. 4, there is no clear peak of the thermal shock wave and a step-type wave front is observed in this case. However, the temperature gradient from the deepest position of heat conduction region to the step-type peak, where $T = 738.722$ and 691.228 K in Fig. 4, respectively, is smooth and a steep gradient in front of the wave is not clearly formed as a result of heat conduction. In Fig. 2, another compressive region can be observed clearly at the back of the thermal shock wave. This can be also observed in Fig. 3 slightly. This region shows a rarefaction wave and it appears as a result of elastic release at the front of the thermal shock wave. In Case 3, the propagation velocity of the thermal shock wave is about 7400 m/s. The rarefaction wave propagates toward a direction opposite to that of propagation of the thermal shock wave. In this case, thus, the rarefaction wave is canceled by the thermal shock wave because the propagation velocity is very fast. Regarding other characteristics shown in Fig. 4, a remarkable temperature rise can be observed out of laser diameter at the surface. This reason can be seen in Fig. 5. Fig. 5 shows snapshots of temperature distribution for the total calculation system. In Fig. 5, (a) is Case 1 at 1.0 ns, (b) is Case 2 at 1.0 ns and (c) is Case 3 at 0.76 ns, and a number of the contour line for a temperature and the display range of the contour line is shown in each figure. As shown in Fig. 5, it is found that an ablation occurs and a surface region irradiated by a pulsed laser is emitted to an air region with phase changes, which are melting and evaporation. The emitted surface material is called a plume. In Case

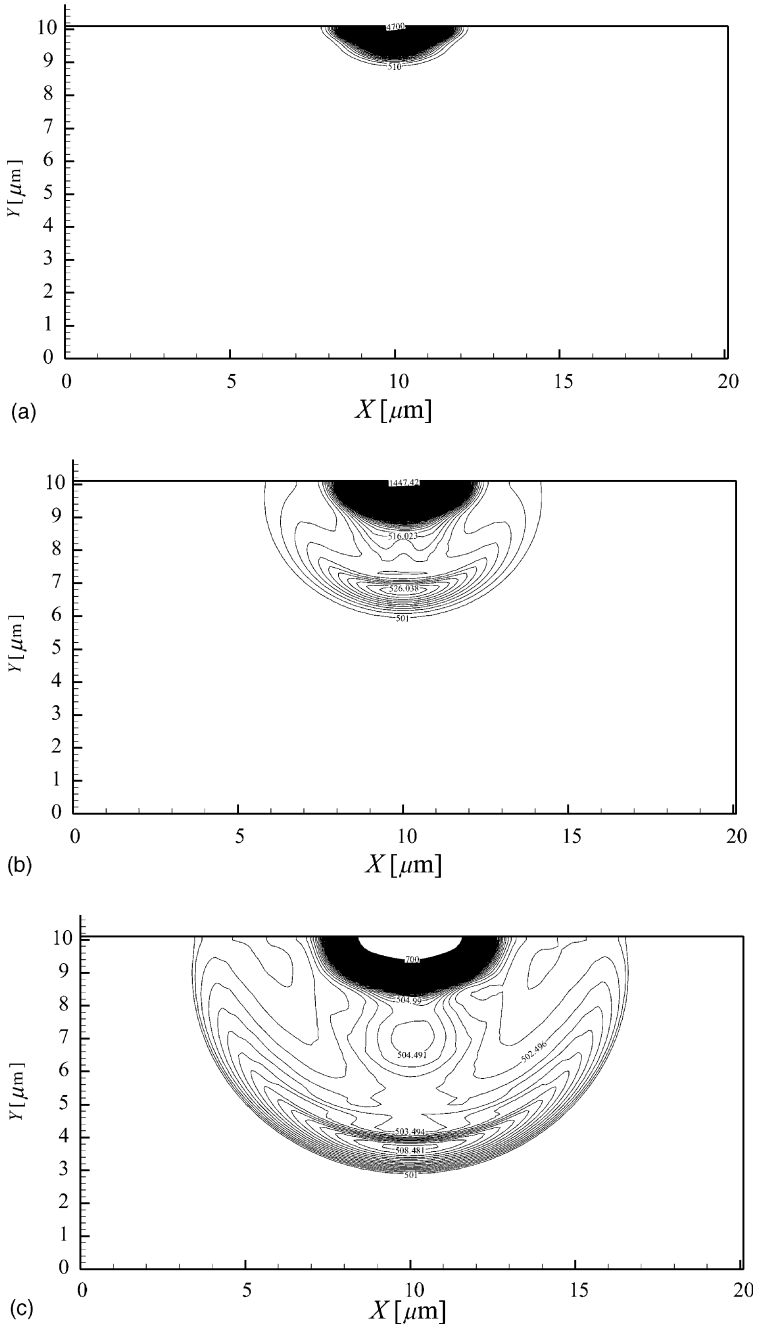

Fig. 2. Temperature distribution within an aluminum thin foil in Case 1, in which $t_p = 1.0$ ps and $I_0 = 5.0 \times 10^{16}$ W/m^2. (a) 0.1 ns and $T = 510$–4700 K, (b) 0.5 ns and $T = 501$–1500 K, (c) 1.0 ns and $T = 501$–700 K.

3, the plume is spread to the X-direction, which is a radius direction, and the bottom of the plume is in contact with a surface region out of a laser irradiation radius. So, the surface region out of the radius is also molten and evaporated as well as the center region irradiated by a pulsed laser as shown in Fig. 4. The thermal expansion time has the time scale required to start the expansion after absorption of the incident laser energy as mentioned above. In this case, since the pulse duration is longer than it, the injection of the laser energy doesn't finish during the laser irradiation. So the laser irradiation to the surface region starting the ex-

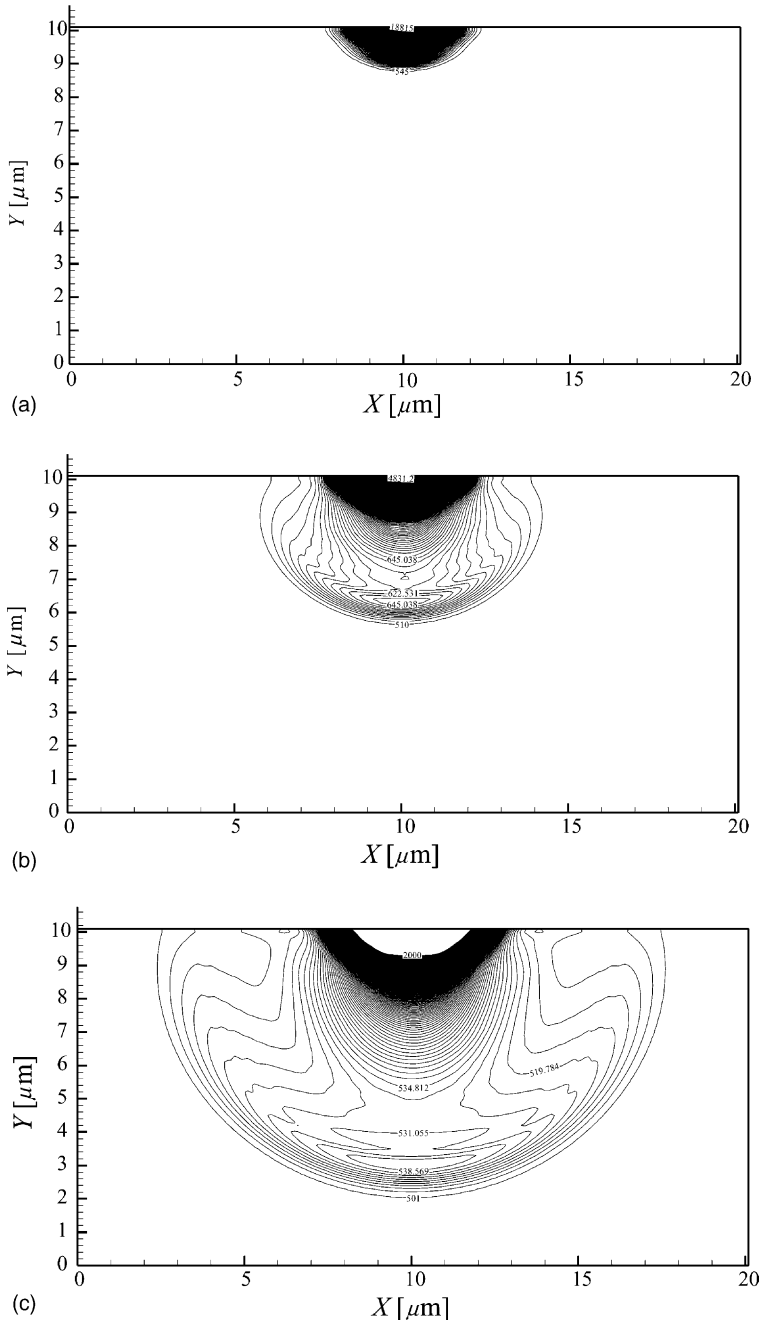

Fig. 3. Temperature distribution within an aluminum thin foil in Case 2, in which $t_p = 10.0$ ps and $I_0 = 5.0 \times 10^{16}$ W/m^2. (a) 0.1 ns and $T = 545$–19,000 K, (b) 0.5 ns and $T = 510$–5000 K, (c) 1.0 ns and $T = 501$–2000 K.

pansion continues and the expansion is accelerated. As a result, the plume spreads to the radius direction.

Fig. 6 shows temperature distributions within a thin foil at 1.0 ns. Case 4 is $t_p = 1.2$ ps, Case 5 is 2.0 ps and Case 6 is 4.0 ps, and $I_0 = 5.0 \times 10^{16}$ W/m^2, respectively. $N_c = 400$ and the display range of the contour line is shown in each figure. With the pulse duration increased, heat conduction can be observed under the region irradiated by laser and the region transferred by heat conduction spreads to the X-direction. Fig. 7 shows a temperature distribution within a thin foil at 1.0 ns. Case 7 is $I_0 = 7.0 \times 10^{16}$ W/m^2, Case 8 is

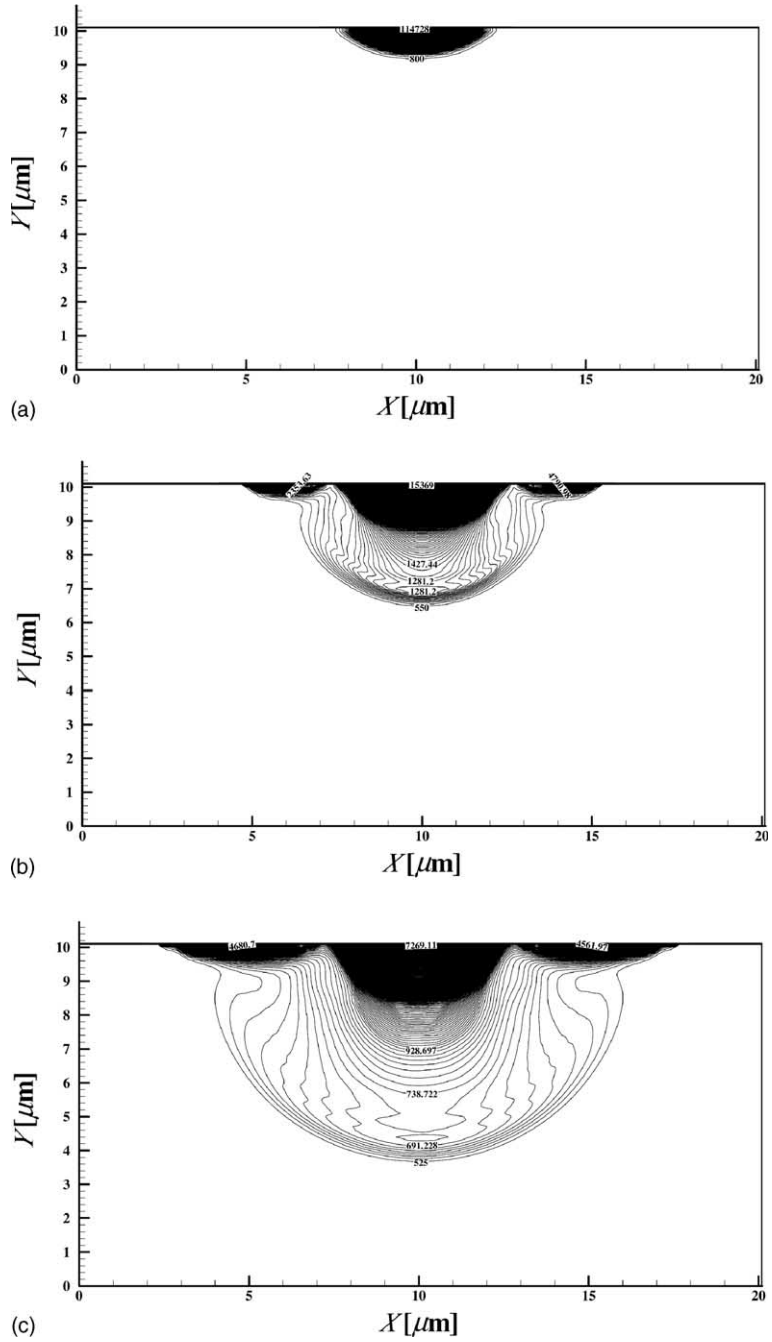

Fig. 4. Temperature distribution within an aluminum thin foil in Case 3, in which $t_p = 100.0$ ps and $I_0 = 5.0 \times 10^{16}$ W/m^2. (a) 0.09 ns and $T = 800$–125,000 K, (b) 0.39 ns and $T = 550$–20,000 K, (c) 0.76 ns and $T = 525$–10,000 K.

1.0×10^{17} W/m^2 and Case 9 is 5.0×10^{17} W/m^2, and $t_p = 1.0$ ps, respectively. $N_c = 400$ and the display range of the contour line is shown in each figure. With the laser intensity increased, heat conduction and the spread to the X-direction can be observed as well as in Fig. 6. As shown in Figs. 6(b) and 7(b), the two temperature distributions are almost equal. In both cases, the total incident laser energy density, which can be described by $E_{in} = t_p \times I_0$, is the same value, $E_{in} = 1.0 \times 10^5$ J/m^2. In short, the appearance of pure heat conduction mode can be predicted by the value of E_{in}. Although it is not shown here, heat conduction slightly

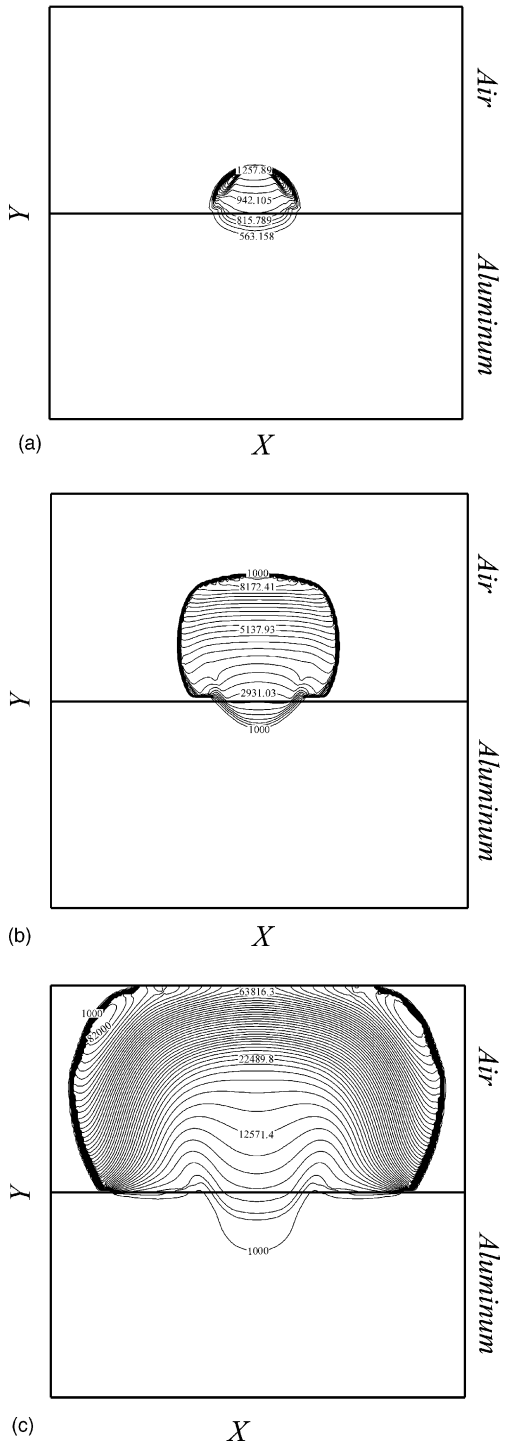

Fig. 5. Temperature distribution for the total calculation system. (a) Case 1 at 1.0 ns, $T = 500$–1700 K and $N_c = 20$; (b) Case 2 at 1.0 ns, $T = 1000$–9000 K and $N_c = 30$; (c) Case 3 at 0.76 ns, $T = 1000$–$82{,}000$ K and $N_c = 50$.

occurred for $t_p = 1.1$ ps and $I_0 = 5.0 \times 10^{16}$ W/m^2 and a temperature distribution for $t_p = 0.5$ ps and $I_0 = 1.0 \times 10^{17}$ W/m^2 was the same as in Fig. 2(c). Therefore, the effect of heat conduction can be ignored when E_{in} have a value under 5.0×10^4 J/m^2. In this paper, however, thermal radiation from a plume is not considered and thus the problem of reheating by a plume cannot be represented. In future work, thermal radiation should be introduced to this simulation. Although the plume is not changed to plasma when E_{in} is small, plasma is generated when E_{in} is large. So, the plasma should be considered in order to perform more accurate analysis of the ablation phenomenon but it need not to be considered for an analysis of the thermal shock wave. It is important to pay attention to E_{in} for the thermal shock wave.

The peak temperature of thermal shock wave does not exceed a melting point of aluminum in every case except for Case 3. Thus, thermal shock wave in these cases has no chance to disturb an internal structure. As a result, in laser processing, if laser with a pulse duration shorter than the characteristic time for pure heat conduction and the total incident energy density of under 5.0×10^4 J/m^2 is used for aluminum, the processing can be performed with more accuracy. Therefore, it can be concluded that the inherent operation parameter of laser processing for each material exists in order to suppress the heat conduction effect and increase the accuracy of processing and is determined by the value of the total incident laser energy density.

In this study, we basically used the Fourier law in our formulation but wave-type heat transfer can be analyzed by our method. Conventionally, for the study of short-pulsed heating phenomena, the two-step model or the DPL model has been used. However, phase change, compressibility and mass transfer are not considered in these models and the convective term is not included in the equations used. Thus, they are unsuitable for analysis of thermal transient phenomena with phase change in materials subjected to irradiation of a high-power short-pulsed laser, which is the subject of the present study. According to our previous work using the molecular dynamics method [30], the wave-type heat transfer phenomenon can be considered to be a highly compressive fluid phenomenon with high density and high pressure, what is referred to as the thermo-mechanical coupling effect. Fig. 8(a)–(c) shows pressure, density and temperature distribution in the center of X-direction, $X = 10$ μm, for Case 1 and Fig. 9 shows the extended diagram of the temperature distribution inside the Al thin foil, which means the region from $Y = 0$ to 10 μm, in the center of X-direction. As shown in Figs. 8(a)–(c) and 9, pressure and density waves propagating toward the inside of Al thin foil with the pressure, density and temperature coupling are observed. The

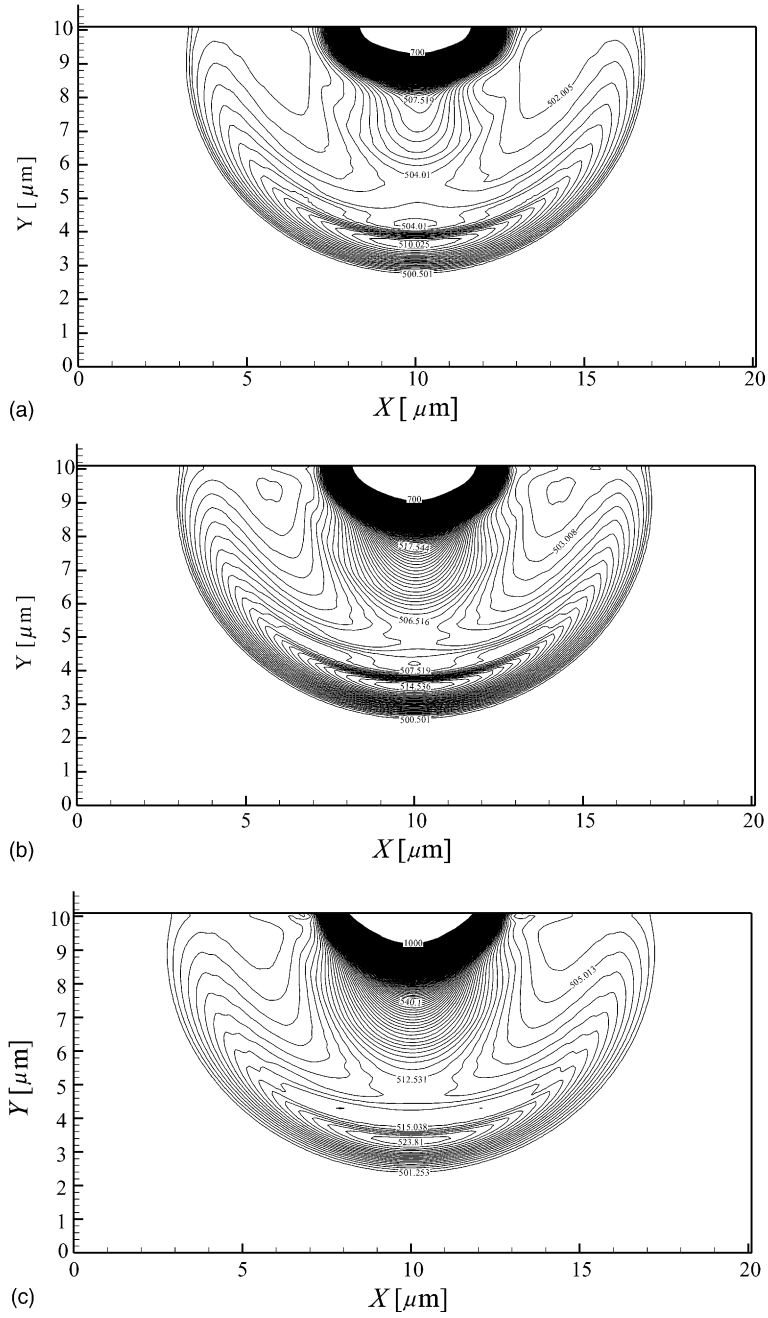

Fig. 6. Temperature distribution within an aluminum thin foil for $I_0 = 5.0 \times 10^{16}$ W/m^2 at 1.0 ns. (a) Case 4, in which $t_p = 1.2$ ps, and $T = 500$–700 K; (b) Case 5, in which $t_p = 2.0$ ps, and $T = 500$–700 K; (c) Case 6, in which $t_p = 4.0$ ps, and $T = 500$–1000 K.

surface temperature rises to about 14000 K but it decreases to about 5000 K after 0.1 ns and about 1000 K after 1.0 ns. Atoms given the laser energy can leave the potential well and approach the neighbor atom. So, the wave-type heat transfer does not occur as a result of heat conduction but as a result of heat transfer with mass transfer. From this point of view, the method using the Fourier law in the equation of energy includes the consistency such that the thermal propagation velocity is infinite, but the thermo-convective model, which con-

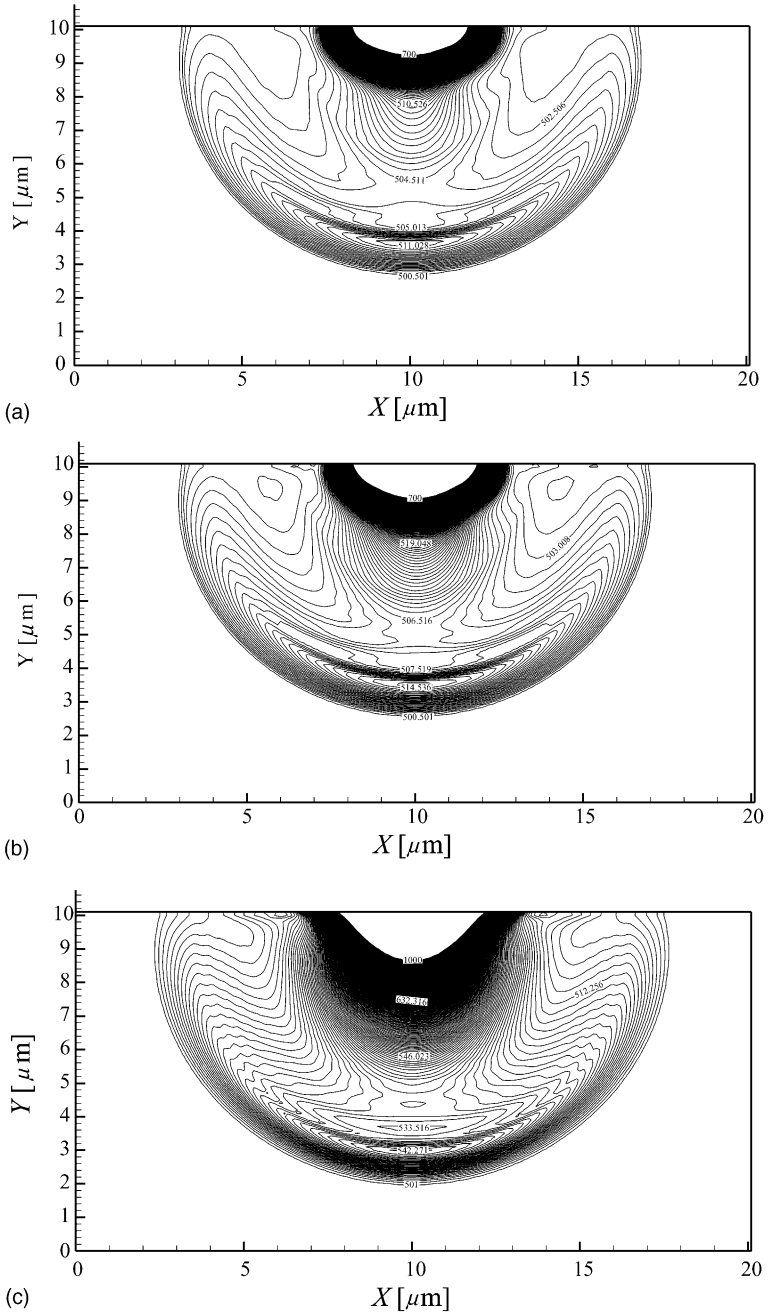

Fig. 7. Temperature distribution within an aluminum thin foil for $t_p = 1.0$ ps at 1.0 ns. (a) Case 7, in which $I_0 = 6.0 \times 10^{16}$ W/m^2, and $T = 500$–700 K; (b) Case 8, in which $I_0 = 1.0 \times 10^{17}$ W/m^2, and $T = 500$–700 K; (c) Case 9, in which $I_0 = 5.0 \times 10^{17}$ W/m^2, and $T = 501$–1000 K.

sists of the equation of continuity, the equation of motion, the equation of energy and the EOS, can describe the wave-type heat transfer since it is a compressive fluid phenomenon.

5. Conclusions

Simulation using the CIP method is performed for the wave-type heat transfer in aluminum thin foil

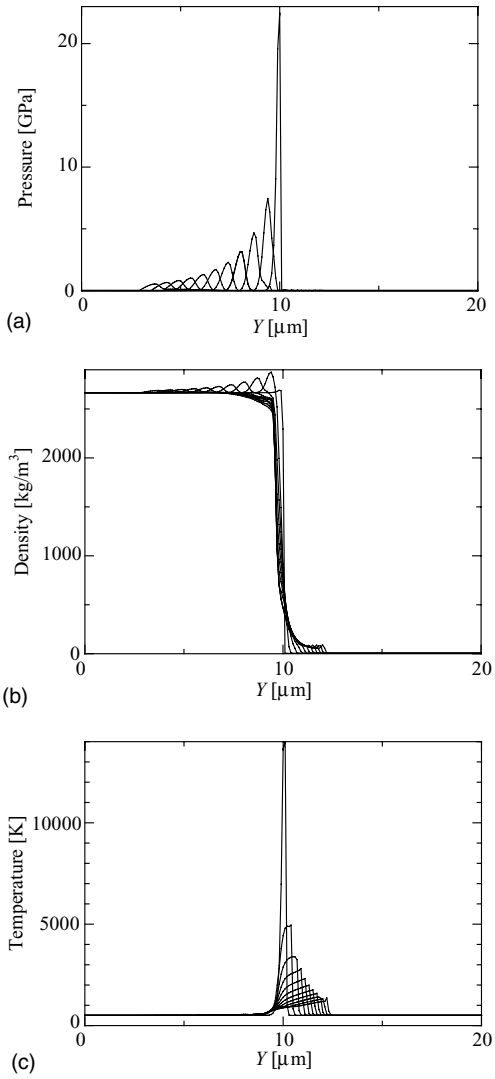

Fig. 8. Pressure, density and temperature distribution in the center of X-direction, $X = 10$ μm, for Case 1. Solid lines in these graphs describe the distribution from 0.1 to 1 ns at 0.1 ns interval. (a) Pressure, (b) density, (c) temperature.

irradiated by a pulsed laser. The results are summarized as follows:

1. When pulse duration is under the order of picosecond, heat conduction is hardly observed and heat transfer toward the inside of aluminum thin foil occurs only by a thermal shock wave. However, heat transfers by conduction if laser fluence is large.
2. The appearance of heat conduction mode after pulse laser irradiation is strongly dependent upon the value of E_{in} and the threshold value to suppress the appearance of heat conduction mode is 5.0×10^4 J/m^2 for aluminum. When the thermal shock wave occurs so as to suppress the heat conduction mode, the wave makes no disturbance in the internal structure.

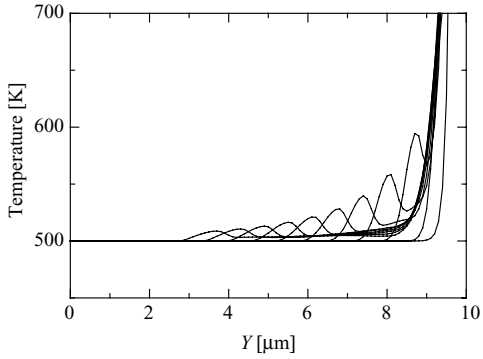

Fig. 9. Extended diagram of temperature distribution inside the Al thin foil, which means the region from $Y = 0$ to 10 μm, in the center of X-direction.

References

[1] C. Cattaneo, Cr. Hebd. Acad. Sci. 247 (4) (1958) 431–433.
[2] P. Vernotte, Cr. Hebd. Acad. Sci. 246 (22) (1958) 3154–3155.
[3] P. Vernotte, Cr. Hebd. Acad. Sci. 247 (23) (1958) 2103–2105.
[4] D.S. Chandrasekharaiah, Appl. Mech. Rev. 39 (3) (1986) 355–376.
[5] D.Y. Tzou, Trans. ASME: J. Heat Transfer 114 (1992) 1042–1045.
[6] M.N. Özisik, D.Y. Tzou, Trans. ASME: J. Heat Transfer 116 (1994) 526–535.
[7] D.Y. Tzou, Trans. ASME: J. Heat Transfer 117 (1995) 8–16.
[8] D.Y. Tzou, in: G.F. Hewitt, C.L. Tien (Eds.), Macro- to Microscale Heat Transfer, Taylor & Francis, 1996.
[9] K. Mitra, S. Kumar, A. Vedavarz, M.K. Moallemi, Trans. ASME: J. Heat Transfer 117 (1995) 568–573.
[10] W. Kaminski, J. Heat Transfer 112 (1990) 555–560.
[11] D. Tang, N. Araki, J. JSME Ser. B 62 (595) (1996) 1136–1141 (in Japanese).
[12] D. Tang, N. Araki, J. JSME Ser. B 62 (604) (1996) 4183–4188 (in Japanese).
[13] D. Tang, N. Araki, Proceedings of 37th National Heat Transfer Symposium, HTSJ, Kobe, Japan, 2000, pp. 897–898 (in Japanese).
[14] N. Sumi, J. JSME Ser. B 64 (625) (1998) 2257–2262 (in Japanese).
[15] H. Ozoe, N. Sato, S.W. Churchill, Chem. Eng. Commun. 5 (1980) 203–221.
[16] S.W. Churchill, M.A. Brown, Int. Commun. Heat Mass Transfer 14 (6) (1987) 647–655.
[17] A.V. Kuznetsov, Int. J. Heat Mass Transfer 37 (18) (1994) 3030–3033.

[18] A.V. Kuznetsov, Int. J. Heat Mass Transfer 40 (5) (1997) 1001–1006.
[19] T. Yabe, T. Ishikawa, P.Y. Wang, T. Aoki, Y. Kadota, F. Ikeda, Comput. Phys. Commun. 66 (1991) 223–242.
[20] T. Yabe, 4th International Seminar "Numerical Analysis of Weldability", Gaz-Seggau, 1997.
[21] S. Fujii, T. Kunugi, T. Utsumi, M. Akamatsu, Proceedings of 11th CFD Symposium, JFCFD, Tokyo Japan, E2-4, 1997 (in Japanese).
[22] T. Utsumi, A. Sasaki, Proceedings of 14th CFD Symposium, JFCFD, Tokyo Japan, D05-3, 2000 (in Japanese).
[23] J.U. Brackbill, D.B. Kothe, C. Zemach, J. Comput. Phys. 100 (1992) 335–354.
[24] T. Yabe, F. Xiao, J. Phys. Soc. Jpn. 62 (8) (1993) 2537–2540.
[25] M.L. Wilkins, in: Calculation of Elastic–Plastic Flow, Methods in Computational Physics, vol. 3, Academic Press, New York, 1964, pp. 211–263.
[26] F. Xiao, T. Yabe, Proceedings of 9th Computational Dynamics Symposium, JSME, Fukuoka Japan, No. 96-25, 438, 1996 (in Japanese).
[27] P. Lyon, J.D. Johnson, LA-UR-92-3407, 1992.
[28] E. Hoashi, T. Yokomine, A. Shimizu, Numer. Heat Transfer Part A 41 (8) (2002) 783–801.
[29] R.B. Oswald Jr., F.B. McLean, D.R. Schallhorn, T.R. Oldham, J. Appl. Phys. 44 (8) (1973) 3563–3574.
[30] E. Hoashi, K. Ezato, T. Kunugi, T. Yokomine, A. Shimizu, Proceedings of CHT'01 Symposium on Advances in Computational Heat Transfer, ICHMT, 2001, pp. 1049–1056.